Available online at www.sciencedirect.com

ScienceDirect

Procedia Structural Integrity 31 (2021) 127–133

Structural Integrity Procedia

www.elsevier.com/locate/procedia

4th International Conference on Structural Integrity and Durability, ICSID 2020

Composite material selection for aircraft structures based on experimental and numerical evaluation of mechanical properties

G. Kastratović[a], A. Grbović[b], A. Sedmak[b], Ž. Božić[c], S. Sedmak[d]*

[a] *Faculty of Transport and Traffic Engineering, University of Belgrade, Vojvode Stepe 305 11000 Belgrade, Serbia*
[b] *Faculty of Mechanical Engineering, University of Belgrade, Kraljice Marije 16, 11120 Belgrade, Serbia*
[c] *University of Zagreb, Faculty of Mech. Eng. And Nav. Arch., I. Lučića 5, 10000 Zagreb, Croatia*
[c] *Innovation Centre of Faculty of Mechanical Engineering, Kraljice Marije 16, 11120 Belgrade, Serbia*

Abstract

In this paper determination of mechanical properties of composite material using experimental and numerical approach is presented. The mechanical properties of a laminate obtained in the experiment are used for verification of numerically obtained values, as well as estimation of the load-carrying capacities of composite engine cover of light aircraft. Composite specimens, consisting of epoxy matrix and glass fibers with orientation angles 0^o, 45^0, and 90^0, have been made according to standards, and the mechanical properties were investigated in tensile and three-point bending tests. The tensile strength, bending strength, elasticity modulus, strain, and force at laminate failure have been evaluated and then compared to values obtained in numerical simulations with the aim of verifying the FE model used for failure prediction of structural laminates. Good agreement of experimental and numerical values provides a solid foundation for further improvements of the numerical model.

Keywords: Composite; Mechanical properties; Multilayered laminate; Fiber orientation angle.

1. Introduction

Composites have excellent mechanical properties and provide the ability to improve structures and materials at the same time. Compared to common materials, they can have noticeably improved strength, stiffness, corrosion, wear, and fatigue resistance, which is crucial when designing components of an aircraft. The composite material must be

* Corresponding author.
E-mail address: simon.sedmak@yahoo.com (S. Sedmak)

2452-3216
10.1016/j.prostr.2021.03.021

designed so its mechanical properties are adjusted to its use, i.e. the exploitation conditions. According to Lopresto et al. (2017), Xia et al. (2001), Hu et al. (2015), and other researchers, the mechanical properties of fiber-reinforced composites considerably depend on the appropriate choice of volume fraction, fiber orientation, layer sequence, and fiber distribution in the matrix. As result, strong and light material is obtained, suitable for application in various industries, even in civil engineering (Kožar et al. (2019) and (2020)). Because of their unique properties and increasing use nowadays, Liu, H. et al. (2020) investigated the behaviour of composites subjected to impact loading. It is well known that the aircraft industry is the leading industry in terms of the implementation of new materials and technologies, and two main approaches are used in the development of airframe structures. The first one, favoured by many researchers (Sghayer et al. (2017), Grbović et al. (2019), Solob et al. (2020), Đukić et al. (2020), Božić et al. (2014) and (2018)) is focused on the improvement of existing materials and designs, while the second approach implies the application of newly developed composite materials (Castanie et Al. (2020)). When it comes to aircraft structures, the chosen materials must have adequate strength and stiffness in accordance with the presumed load. Proper evaluation of composite mechanical properties is of utmost importance in order to ensure the safe and long-term use of airframe structures.

During the development of the light aircraft "Owl", it was decided to design a composite engine cover and compare its load-carrying capabilities with traditional aluminium alloy cover. To obtain mechanical properties of newly designed composite laminate, extensive testing was carried out along with the numerical simulations of the specimen's behaviour under the same loads. The most important results are presented in this paper.

2. Material

Test specimens have been made of multi-layered composite (laminate) with fiber orientation angles most commonly used in practice (0°, 45°, and 90°). The lamina (Fig. 1) consisted of fiberglass (type: weaving) and Araldit M epoxy resin, with a hardener of type HY-956.

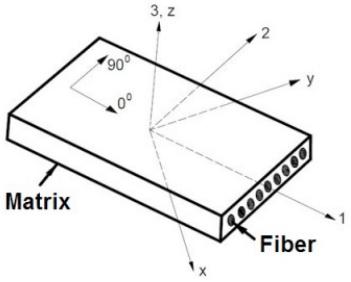

Fig. 1. Fiber orientation relative to the matrix.

Table 1. Mechanical properties of weaving.

Property	Value	Unit
Fibers density	2500	[kg/m^3]
Thickness of layer (dry)	0.18	[mm]
Surface mass	163	[g/m^2]
Tensile strength	335	[MPa]
Young elasticity modulus E_1	19	[GPa]
Young elasticity modulus E_2	18	[GPa]
Poisson coefficient ν	0.22	-
Shear strength F_{12}	50	[MPa]
Shear strength F_{21}	45	[MPa]
Bending strength F_{11}	495	[GPa]
Bending strength F_{22}	460	[GPa]

The fiberglass was twilled perpendicularly (θ_1=0°, θ_2=90°), and was produced by Interglas manufacturer in accordance with standard 8.4548.60 and LN9169. The most important properties of the composite components, as well as calculated properties of lamina, are presented in tables 1– 4.

Table 2. Chemical composition of the glass.

Chemical composition	Share [%]
Silicon-oxide	52-56
Aluminium (III)-oxide	12-16
Boron (III)-oxide	5-10
Sodium (I)-oxide and Potassium(I)-oxide	0-2
Magnesium (II)-oxide	0-5
Calcium (I)-oxide	16-25
Titanium (IV)-oxide	0-1.5
Iron (III)-oxide	0-0.8
Iron	0.1

Table 3. Mechanical properties of mixed resin.

Property	Value	Unit
Density	1200	[kg/m^3]
Tensile strength, Rm	55-65	[MPa]
Elongation, ε	3-4	[%]
Tensile elasticity modulus, E	2.5-2.8	[GPa]
Tensile strength, R_F	85-100	[MPa]
Bending elasticity modulus, E	3-3.3	[GPa]

Table 4. Evaluated mechanical properties of lamina.

Property	Value	Unit
Young elasticity modulus E_1	10.62	[GPa]
Young elasticity modulus E_2	10.62	[GPa]
Poisson coefficient ν_{12}	0.28	-
Tensile strength, F_{1T}	222.86	[MPa]
Elongation, ε	2.95	[%]
Plain shear modulus, G_{12}	2.95	[GPa]
Interlaminar shear modulus, G_{23}=G_{13}	2.86	[GPa]

3. Experimental investigation

Tests presented in this paper were carried out in accordance with ASTM 3039 standard (tensile tests) and ASTM 7264 (three-point bending tests). Details regarding these standards can be found in ASTM D7264/D7264M-15. Dimensions of the test specimens used are 250 x 25 x 2.5 mm (Fig. 2). Ten specimens for each fiber orientation angle (0°, 45°, and 90°) have been made (in total 30) and tested at the standard room temperature (t=20°C): fifteen with tensile load and fifteen using a bending load. Tests were carried out on electro-mechanical testing machine SCHENK TREBEL RM 200, Fig. 3(a).

During the tensile tests, force F and elongation Δl were continually recorded. The range of extensometer measurement was +2,5mm (accuracy $\pm$0.05 mm). During three-point bending tests applied force P was continuously monitored, as well as the deflection δ of the specimen, with the same range of extensometer measurement +2,5mm (accuracy$\pm$0.05 mm).

Here, experimental values obtained in tensile and bending tests of specimens with fiber orientation angle 0^0 will be presented. Then, the tensile test results will be compared to equivalent numerical values for the purpose of FE model verification.

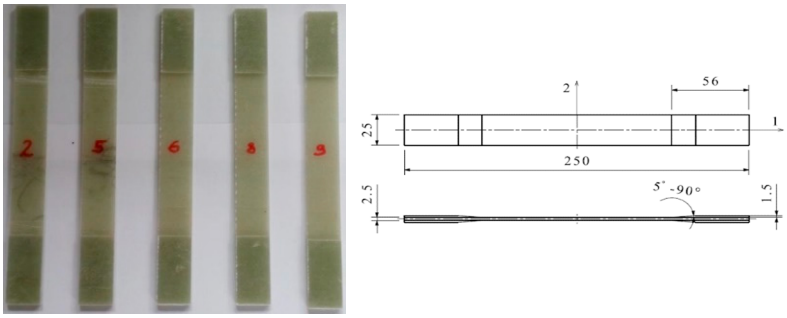

Fig. 2. Test specimen geometry and dimensions.

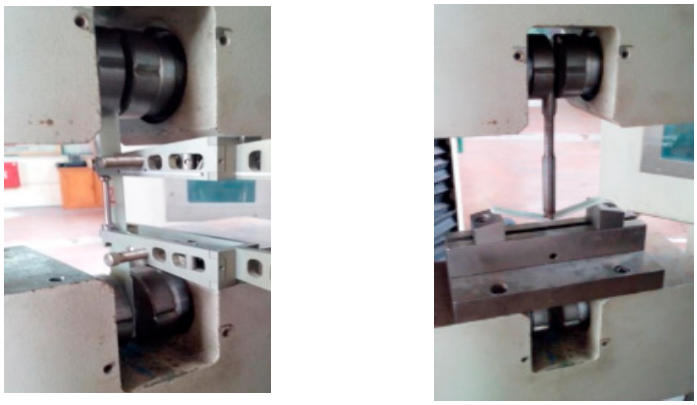

(a) (b)

Fig. 3. Electro-mechanical testing machine SCHENK TREBEL RM 200: (a) tensile test; (b) three-point bending test.

4. Experimental results

Results of the tensile tests are presented in Table 5, where MV stands for mean value, SD stands for standard deviation, and CV stands for coefficient of variation. Mechanical properties obtained in tensile tests with 5 specimens show the small spread of values around calculated means, while only in the case of specimen K-2 value of strain at failure is significantly different from other values (Fig. 4(a)). If values obtained with specimen K-2 are omitted, somewhat lower mean values are obtained (E_T = 11.61 GPa, R_m = 209.29 MPa, and ε = 2.22%). As Figure 4(b) shows all fractures occurred near grip sections of specimens.

Table 5. Tensile test results (Elasticity modulus E_T, force F, tensile strength R_m, and strain ε).

Specimen	E_T [GPa]	F [daN]	R_m [MPa]	ε [%]
K-2	12.5	1355.13	218.73	3.17
K-5	12.5	1300.91	217.55	2.28
K-6	11.35	1294.49	208.25	2.21
K-8	11.25	1300.72	204.29	2.19
K-9	11.34	1256.30	207.07	2.21
MV	11.79	1301.51	211.18	2.41
SD	0.65	35.25	6.53	0.42
CV [%]	5.52	2.71	3.09	17.57

Specimen K-2 showed notably different value of strain at failure, while modulus of elasticity was – after some variations between ε=0.5% and ε=1.5% – comparable to values obtained with other 4 specimens (anyhow, graph in Fig. 4(a) justifies the exclusion of results obtained with K-2). On the other hand, it can be recognized from fractured specimens (Fig. 4 (b)) that brittle fracture of glass/polymer composite systems occurred.

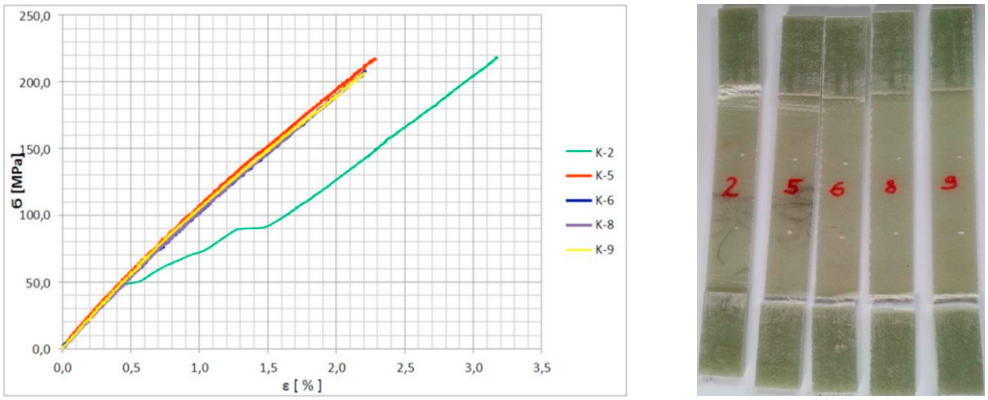

(a) (b)

Fig. 4. (a) Stress-strain diagrams for tested specimens (tensile test); (b) Tensile test specimens' fracture.

Results of the three-point bending tests are presented in Tab. 6 and Fig 5(a).

Table 6. Three-point bending test results (Elastic modulus E_F, force P, Normal bending stress σ_s, deflection δ and strain ε).

Test bars, n=5	Efc [GPa]	P [daN]	σ_s [MPa]	δ [mm]	ε [%]
KC-4	9.32	32.82	252.46	15.40	3.27
KC-5	11.10	34.78	267.54	14.01	2.96
KC-6	11.02	34.59	266.08	14.16	2.99
KC-7	11.42	35.58	273.69	14.03	2.96
KC-8	10.58	32.30	248.46	13.79	2.91
MV	10.69	34.01	261.65	14.28	3.02
SD	0.82	1.39	10.70	0.64	0.14
CV [%]	7.65	4.09	4.09	4.49	4.79

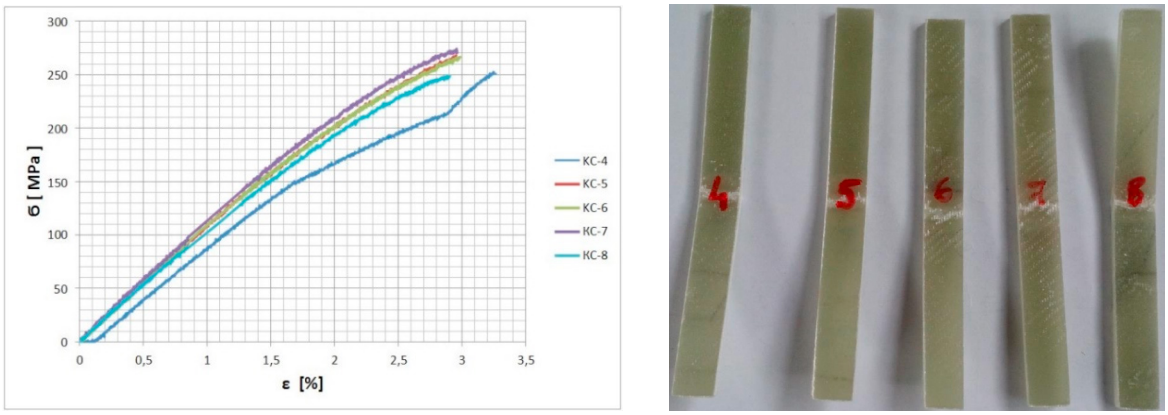

(a) (b)

Fig. 5. (a) Stress-strain diagrams for tested specimens (three-point bending); (b) Bending test specimens' fracture.

Fig. 5(a) shows that specimen KC-4 "produced" considerable deviation in strain values compared to other specimens (similarly to K-2 specimen in tensile experiment). By omitting the values obtained with K-4, the following mean values are obtained: $E_F = 11.03$ GPa, $R_m = 263.94$ MPa, and $\varepsilon = 2.95\%$. The fractured specimens can be seen in Fig. 5(b). Fractures occurred in the middle of the specimens, as expected.

5. Numerical simulation and comparison of results

To carry out numerical simulation of tensile test of the composite specimen, a structural model of the specimen was created in ANSYS APDL. The analysis was set up, including the mesh, material, boundary conditions, and loads. The model was then imported into the module Advanced Material Exchange (AME), which is part of Autodesk Helius PFA software. Within AME the fiber orientations and the residual strains are mapped from the Moldflow model to the structural model which is then exported to Ansys with the modified material definition. The .hin extension file (Helius input file) controls the damage evolution criteria, while the .sif extension file (structural interface file) contains the mapped fiber orientations and the Ramberg-Osgood material information.

Fig. 6(a) shows that in FE simulation the rupture occurs in the same place as in tensile load experiments (red areas). A value of 1.0 indicates an undegraded material (no failure) while a value of 2.0 indicates the Gauss point location has failed and the material stiffnesses have been degraded. Fig. 6(b) shows the tangent elastic modulus of the matrix material. When the tangent stiffness decreases, the structure is undergoing plastic deformation, or softening. After calculations in Ansys (Fig. 6), a set of post-processing commands can be used to automatically extracts the load-displacement response from the results file and create a stress-strain plot (Fig. 7).

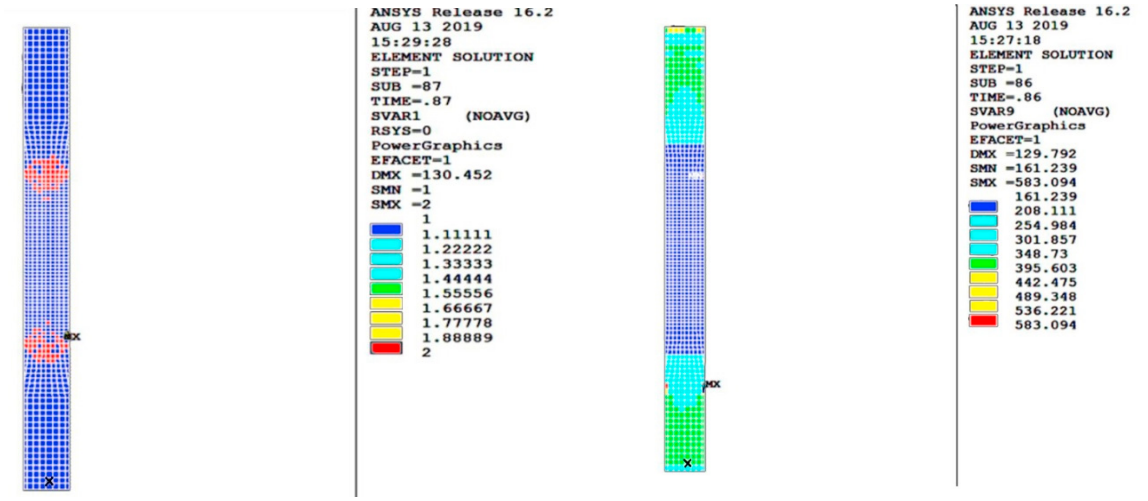

Fig. 6. Finite element analysis of composite specimen-tensile load: (a) Rupture state; (b) Matrix tangent elastic modulus.

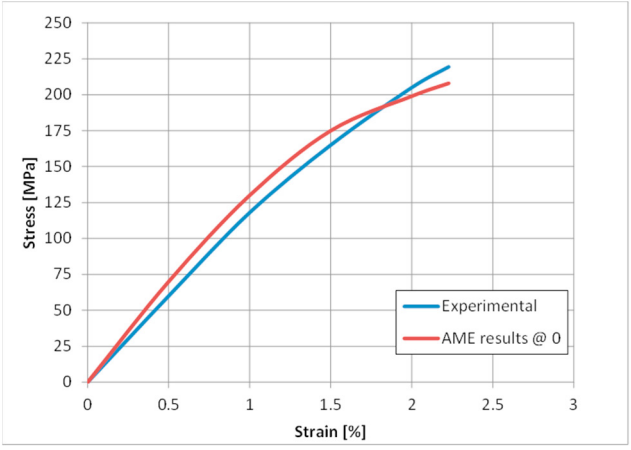

Fig. 7. Comparison of the numerically and experimentally obtained results for fiber orientation angle 0°

Results obtained in numerical simulations are compared to results obtained in the experimental investigation (Fig. 7). A good fit was achieved, which confirms the validity of the numerical model with fiber orientation angle 0^0 when a tensile load is applied.

6. Conclusion

The main goals of the presented investigation were to determine the mechanical properties of designed fiberglass reinforced epoxy and evaluate/verify the developed numerical model. According to results obtained in experiments with specimens, designed material can be used for the production of aircraft engine cover since CFD analysis (not presented in this paper) revealed that maximum stress on the cover during the flight is far below the tensile strength of the designed material. The numerical model of specimen developed in AME software provided satisfactory values that are comparable to experimental results. The methodology used to design the numerical model and conducted calculations can be now used to design more complex geometry of aircraft structural components and evaluate their integrity without the need for expensive full-scale tests.

Acknowledgements

The authors from Serbia would like to thank the Ministry of Education, Science and Technological Development of the Republic of Serbia for financial support.

References

ASTM D7264 / D7264M-15, Standard Test Method for Flexural Properties of Polymer Matrix Composite Materials, ASTM International, West Conshohocken, PA, 2015, www.astm.org

Božić Ž., Schmauder S., Mlikota M. and Hummel M., 2014. Multiscale fatigue crack growth modelling for welded stiffened panels. Fatigue and Fracture of Engineering Materials and Structures 37(9), 1043-1054.

Božić Ž., Schmauder S. Wolf H., 2018. The effect of residual stresses on fatigue crack propagation in welded stiffened panels. Engineering Failure Analysis 84, 346–35.

Castanie, B., Bouvet, C., and Ginot, M. 2020. Review of composite sandwich structure in aeronautic applications, Composites Part C: Open Access 1, 100004.

Đukić, D., Grbović, A., Kastratović, G., Vidanović, N., Sedmak, A., 2020. Stress intensity factors numerical calculations for two penny shaped cracks in the elastic solid. Engineering Failure Analysis 112, 104507.

Grbović, A., Sedmak, A., Kastratović, G., Petrašinović, D., Vidanović, N., Sghayer, A., 2019. Effect of laser beam welded reinforcement on integral skin panel fatigue life. Engineering Failure Analysis 101, 389-393.

Hu, T., et al., 2015. Electromagnetic shielding properties of carbon fiber felt-glass fiber belt multilayer composites with different layer angle. Materials Letters 153(15), 20-23.

Kožar, I., Torić Malić, N., Simonetti, D., Smolčić, Ž., 2019. Bond-slip parameter estimation in fiber reinforced concrete at failure using inverse stochastic model. Engineering Failure Analysis 104, 84-95.

Kožar, I., Torić Malić, N., Simonetti, D., Božić Ž., 2020. Stochastic properties of bond-slip parameters at fibre pull-out. Engineering Failure Analysis 111, 104478.

Liu, H. et al, 2020, The behaviour of fibre-reinforced composites subjected to a soft impact-loading: An experimental and numerical study. Engineering Failure Analysis 111, 104448.

Lopresto, V., Langella, A., Abrate, S., 2017. Dynamic response and failure of composite materials and structures. Duxford-Woodhead publishing.

Sghayer, A., Grbović, A., Sedmak, A., Dinulović, M., Doncheva, E., Petrovski, B., 2017. Fatigue Life Analysis of the Integral Skin-Stringer Panel Using XFEM. Structural Integrity and Life 17, 8-11.

Solob, A., Grbović, A., Božić, Ž., Sedmak, S.A. 2020. XFEM based analysis of fatigue crack growth in damaged wing-fuselage attachment lug. Engineering Failure Analysis 112, 104516.

Xia, M., et al., 2001. Analysis of multi-layered filament-wound composite pipes under internal pressure. Composite structures 53(4), 483-491.